

Crystal structure of the ribosome recycling factor bound to the ribosome

Albert Weixlbaumer¹, Sabine Petry^{1,3}, Christine M Dunham^{1,3}, Maria Selmer¹⁻³, Ann C Kelley¹ & V Ramakrishnan¹

In bacteria, disassembly of the ribosome at the end of translation is facilitated by an essential protein factor termed ribosome recycling factor (RRF), which works in concert with elongation factor G. Here we describe the crystal structure of the *Thermus thermophilus* RRF bound to a 70S ribosomal complex containing a stop codon in the A site, a transfer RNA anticodon stem-loop in the P site and tRNA^{fMet} in the E site. The work demonstrates that structures of translation factors bound to 70S ribosomes can be determined at reasonably high resolution. Contrary to earlier reports, we did not observe any RRF-induced changes in bridges connecting the two subunits. This suggests that such changes are not a direct requirement for or consequence of RRF binding but possibly arise from the subsequent stabilization of a hybrid state of the ribosome.

After termination of protein synthesis and release of the polypeptide chain, the ribosome is left with an empty A site and a deacylated tRNA in the P site. For the ribosome to start another round of translation, this complex needs to dissociate to allow binding of the 30S subunit with initiation factors at the translation start site of messenger RNA. In bacteria, it has been shown that this disassembly is an active process that requires RRF^{1,2}, which works in concert with elongation factor G (EF-G)³.

The crystal structure of RRF⁴ shows that the factor consists of two distinct domains. Domain 1 is a three-helix bundle ($\alpha 1$, $\alpha 3$ and $\alpha 4$), whereas domain 2 has a three-layered $\beta/\alpha/\beta$ structure (Fig. 1). The domains are connected by two flexible linkers. A comparison of the various crystal structures of RRF from different species suggests that domain II is quite mobile and can rotate around an axis formed by the three-helix bundle of domain I⁵⁻⁷. This has been demonstrated more directly by a solution structure of RRF⁸ and by NMR relaxation experiments and molecular dynamics simulations, which suggest that the range of rotation is at least 30° (refs. 8,9).

Because its overall shape and dimensions resemble those of tRNA, it was initially proposed that RRF acts as a tRNA mimic, disassembling the ribosomal subunits through an EF-G-catalyzed translocation of RRF itself⁴. However, subsequent data from directed hydroxyl radical probing of 16S and 23S RNA¹⁰, cryo-EM studies^{11,12} and a crystal structure of domain I bound to the *Deinococcus radiodurans* 50S ribosomal subunit¹³ show that the orientation of RRF in the ribosome is very different from that predicted by the tRNA-mimicry hypothesis.

Genetic studies using heterologous RRF and EF-G from *Escherichia coli* and *Mycobacterium tuberculosis* have suggested a direct interaction between the two factors¹⁴. Mutational studies have mapped this

interaction to the elbow region of RRF and domains IV and V of EF-G¹⁵, and more recently it has been shown that domain II of RRF is important for this interaction¹⁶.

There has been some debate about the mechanism of action of RRF and EF-G in recycling. Originally, it was proposed that the action of RRF and EF-G results in release of the ribosomes from the mRNA¹⁷. Later, it was thought RRF and EF-G act by dissociating the ribosomal subunits, and the deacylated tRNA is then released when initiation factor IF3 binds the 30S subunit¹⁸. However, a subsequent study suggested that release of tRNA and mRNA does not require dissociation of the subunits or the involvement of IF3 (ref. 19). More recent detailed kinetic studies have shown that the dissociation of subunits precedes tRNA release, which requires IF3. Notably, although the disassembly requires GTP hydrolysis by EF-G, there does not seem to be a translocation-like movement of mRNA and tRNA, as is typically associated with EF-G action²⁰.

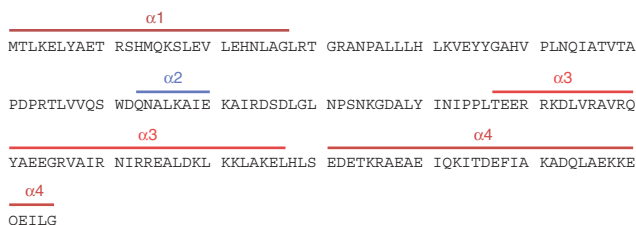
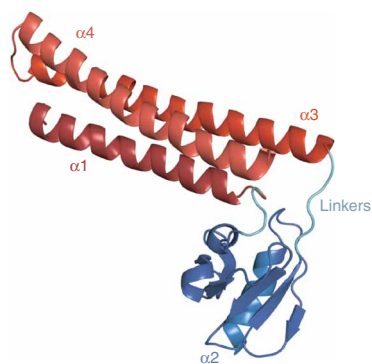
Here we report the crystal structure of *T. thermophilus* RRF bound to a complex of the 70S ribosome with an mRNA that has a stop codon in the A site, a tRNA^{Phe} anticodon stem-loop (ASL^{Phe}) in the P site and cognate tRNA^{fMet} in the E site. The structure allows us to discuss details of the interactions of RRF with the 70S ribosome in the context of previous structural and functional work on ribosome recycling. It also shows that complexes between the ribosome and translation factors can be studied at a sufficiently high resolution to obtain a properly refined crystallographic model.

RESULTS

The crystal form that yielded a high-resolution structure of the *T. thermophilus* 70S ribosome²¹ was used as the basis for determining

¹MRC Laboratory of Molecular Biology, Hills Road, Cambridge CB2 0QH, UK. ²Present address: Department of Cell and Molecular Biology, Uppsala University, Biomedical Center, Box 596, SE-75124 Uppsala, Sweden. ³These authors contributed equally to this work. Correspondence should be addressed to V.R. (ramak@mrc-lmb.cam.ac.uk).

Received 11 June; accepted 28 June; published online 29 July 2007; doi:10.1038/nsmb1282



the structure of a complex of the ribosome with RRF. Well-diffracting crystals of the complex could be obtained by soaking RRF into preformed crystals of the ribosome with ASL^{Phe} in the P site, full-length tRNA^{Met} in the E site and an mRNA with a stop codon in the A site. Crystals diffracting to $\sim 3\text{-}\text{\AA}$ resolution could be obtained reproducibly; but in the crystals obtained so far, crystal mosaicity limited usable data to about $3.5\text{-}\text{\AA}$. Here we report results from a data set refined to $3.5\text{-}\text{\AA}$ resolution (with $I/\sigma I = 2$ at $3.8\text{-}\text{\AA}$), which yielded clearly interpretable electron density maps, owing to the high redundancy and completeness of the data.

Clear density for RRF domain I, as well as mRNA and ASL^{Phe} in the P site, was visible in difference Fourier maps after the first round of refinement with the empty 70S ribosome as the model (Fig. 2a and Supplementary Fig. 1 online). The crystal structure of *T. thermophilus* RRF was used for placement of domain I into the electron density, and adjustments of only side-chain conformations were necessary⁶. The maps were very noisy in the region where domain II would be located, suggesting that although domain I

Figure 2 RRF orientation in the ribosome.

(a) Stereo view of unbiased difference Fourier maps ($F_o - F_c$) for RRF (orange backbone). Domain I is clearly visible, but the map is very noisy in the region where domain II is located. (b) Stereo view of difference Fourier maps calculated to $6\text{-}\text{\AA}$, in which helical parts of domain II become visible. (c) Overall orientation of RRF in the ribosome, with domain I spanning the 50S subunit's A and P sites. ASL^{Phe} is in the 30S subunit's P-site, and tRNA^{Met} occupies the E site. Ribosomal proteins are shown in darker colors, and the mRNA is in magenta. (d) The tip of RRF would clash with a tRNA in the P/P state (modeled using the P-site ASL^{Phe}) but would be compatible with a P/E hybrid state.

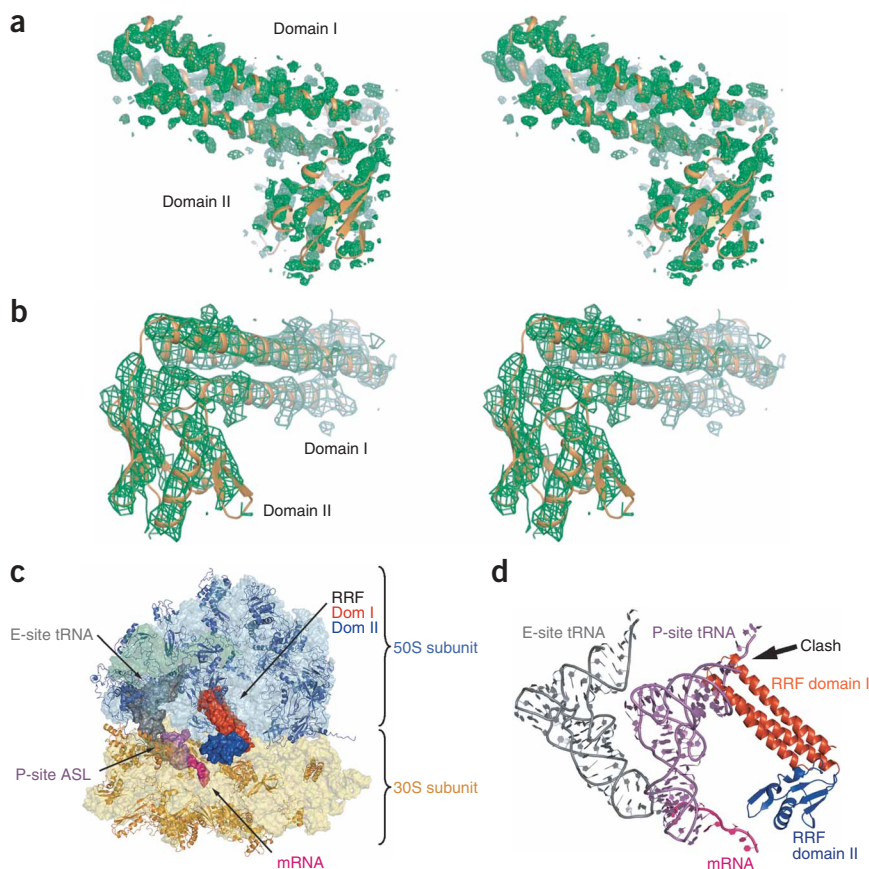


Figure 1 Domain organization of *T. thermophilus* RRF in the ribosome^{4–7}. Domain I, comprising residues 1–29 and 107–185, forms a three-helix bundle (red). Domain II, formed by residues 34–102, has a three-layered β/α structure (blue), and its orientation relative to domain I is shown as it appears in the present complex with the 70S ribosome. Below, sequence of *T. thermophilus* RRF, with α -helices indicated.

is well-ordered by its interactions with the ribosome, domain II is not similarly constrained. Nevertheless, difference Fourier maps calculated to lower resolution showed weak density for helical regions of domain II (Fig. 2b). This allowed us to place domain II and crystallographically refine it as a rigid body.

Notably, crystals of a complex of RRF with a ribosome containing full-length tRNAs in the P and E sites never diffracted to better than $5.5\text{-}\text{\AA}$. Low-resolution maps generated from these crystals (data not shown) indicated that RRF was not bound. Similarly, soaking RRF into preformed crystals of the ribosome containing deacylated tRNAs in both the P and E sites also resulted in loss of high-resolution diffraction.

Interactions of RRF with the ribosome

Figure 2c shows the overall orientation of RRF in the ribosome. Domain I spans the A and P sites on the 50S subunit. This position is incompatible with tRNA in the canonical P/P state because RRF would clash with the acceptor arm of tRNA in the P site (Fig. 2d).

The three-helix bundle of domain I of RRF makes a number of interactions with 23S RNA in the 50S subunit. The tip, formed by the N-terminal residues as well as the loop connecting helix $\alpha 3$ with $\alpha 4$, is located close to the peptidyl transferase center and contacts the P loop of 23S RNA (the P loop spans residues 2246–2258 in *E. coli*).

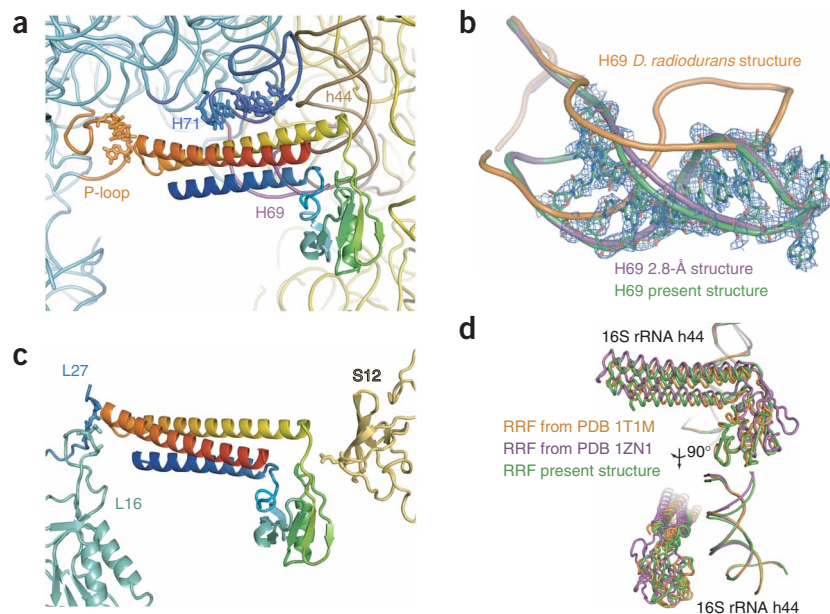


Figure 3 RRF contacts the 70S ribosome. (a) RNA residues within 3.6 Å of RRF in the present structure are shown as sticks. There seems to be no direct contact to H69. Elements of 23S and 16S RNA are highlighted. (b) Simulated annealing omit map for H69. Conformation of H69 in the present structure is very similar to that seen in the high-resolution 70S ribosome structure²¹ without RRF, but different from the structure of *D. radiodurans* 50S subunit¹³ bound to domain I of RRF. (c) Ribosomal protein residues in L16, L27 and S12 that are close enough for contacts to RRF (within 3.6 Å) are shown as sticks. (d) Comparison of RRF orientations in the ribosome in our crystal structure and in previous cryo-EM studies^{11,12} (see text for details).

In addition, helix $\alpha 3$ in RRF domain I makes several contacts to 23S RNA helix 71 (H71) (Fig. 3a). Helix 69 (H69) of 23S RNA in the crystal structure reported here has an essentially identical conformation to that seen in the 70S ribosome without RRF²¹ (Fig. 3b). Moreover, in the present structure, RRF and H69 are not close enough to form direct contacts. Finally, we also do not see any change in the inter-subunit bridges. No contacts to 16S RNA are made, and protein S12 is the only component of the 30S subunit close enough for potential interactions.

Just three ribosomal proteins are within 4 Å of RRF (Fig. 3c). Ribosomal proteins L16 and L27 are in close proximity to the tip of RRF domain I, whereas ribosomal protein S12 is close to the C-terminal end of helix $\alpha 2$ in domain II of RRF. Protein L27 from the large ribosomal subunit has been reported to make a number of contacts with RRF¹³. However, the conformation of the N terminus of L27 in that report is different from the one observed subsequently in the 2.8-Å-resolution structure of the 70S ribosome²¹, where the N terminus is close to the CCA end of P-site tRNA. This location is in agreement with genetic and biochemical data, supporting the influence of L27 on the catalysis of peptide-bond formation²². In contrast, the conformation of the N-terminal residues of L27 seen in *D. radiodurans* would clash with P-site tRNA. This portion of L27 would have to undergo an approximately 90° rotation upon RRF binding, and it is not clear whether this is feasible. In the present structure, density for the backbone of residues 1–10 is only partially visible, but the main chain trace is similar to that of the 2.8-Å structure. No clear indications of the side chain positions are apparent, and therefore no detailed interpretation can be made.

When these data are taken together, L16 and L27 seem to be the only ribosomal proteins with roles in the interactions with RRF.

Even though S12 is close to domain II of RRF (Fig. 3c), it is unlikely that there are interactions strong enough to constrain its orientation, as reflected in the high thermal factor for the domain.

RNA ligands in the ribosome

Density for ASL^{Phe} and the codon in the P site was clearly visible (Supplementary Fig. 1). The conformation of the P-site ASL^{Phe} is very similar to that seen in the high-resolution 70S ribosome structure with full-length tRNA^{Met} in the P site (Supplementary Fig. 2 online). However, as stated earlier, RRF would clash with the acceptor arm of P-site tRNA and would require the acceptor arm to move into the E site.

The E site in the current structure contains a cognate tRNA, in contrast to the high-resolution 70S ribosome structure²¹. The density for the E-site tRNA in difference Fourier maps was much weaker than for P-site tRNA or RRF, and backbone density became visible only when maps were calculated to lower resolution, as was done to visualize domain II of RRF (Supplementary Fig. 3 online). The anticodon loop of the tRNA is not very well defined, and it is not apparent whether codon-anticodon base-pairing takes place. However, the E-site codon adopts a different conformation from that observed previously, bringing it

closer to the anticodon of E-site tRNA.

Notably, we could see weak density for an ASL in the A site. In addition to its expected strong binding to the P site, the large excess of ASL appears also to have bound weakly to the A site as a noncognate species, where it does not sterically interfere with RRF binding.

DISCUSSION

The extensive interactions of RRF with the 50S subunit and the lack of contacts to the 30S subunit explains previous observations of high-affinity binding of RRF to the 50S subunit but no binding to 30S subunit⁷. The high mobility of domain II in our structure is consistent with previous findings suggesting relative flexibility between the two domains^{8,9}. It also suggests that interactions with EF-G may be required to constrain domain II in a specific orientation. Biochemical experiments and mutational studies have shown that domain II is important for interaction with EF-G but not with the ribosome itself⁶.

Differences from previous structures

The overall orientation of RRF is consistent with a crystal structure of domain I of RRF in complex with the 50S subunit¹³. It is also similar to previous cryo-EM studies of RRF bound to the ribosome^{11,12}, but the exact orientation and details of interactions are different from these studies.

The orientation of domain II in the crystal structure is generally in agreement with that inferred from the cryo-EM structure of RRF bound to the empty 70S ribosome (PDB 1T1M)¹¹ but is different from that of RRF bound to ribosomes in complex with tRNAs¹² (PDB 1ZNI) (Fig. 3d). For these comparisons, we superposed helix 44 of 16S RNA and calculated the r.m.s. deviation of equivalent RRF C α atoms. The r.m.s. deviation was 3.5 Å with the cryo-EM structure of RRF in

empty ribosomes, and 7.6 Å with the cryo-EM structure of RRF in ribosomes bound to tRNAs. If RRF itself was used for the superposition, the respective r.m.s. deviations were 2.4 and 5.9 Å. The relatively high latter value reflects mainly the difference in the relative orientation of the RRF domains in the two structures. Because of such differences, the contacts reported in these cryo-EM structures differ from those in the present structure. In particular, even though 23S RNA helix 71 (H71) aligns well, the RRF in the cryo-EM reconstruction with full-length tRNA is shifted and would clash with some of the residues in the P loop, given its conformation in the present structure¹².

H69 of 23S RNA is involved in forming the intersubunit bridge B2a^{21,23–25} and has been implicated in translocation. A substantial change in the conformation of H69 is reported in the crystal structure of RRF domain I bound to *D. radiodurans* 50S subunits (Fig. 3b)¹³. The altered conformation of H69 results in a direct interaction of H69 with a conserved element of RRF in the 50S subunit structure¹³. However, this reported conformation of H69 has unusual geometry for an RNA stem-loop, with disrupted and out-of-plane base pairs.

Changes in the conformation of H69 of 23S RNA upon RRF binding have also been reported in both previous cryo-EM structures, even in the absence of bound tRNA ligands^{11,12}. However, the reported changes in the cryo-EM structures are actually different from those in the 50S subunit structure¹³. Coordinates of H69 are available only for one of the two cryo-EM structures in ref. 12, and superposition of H69 from this cryo-EM structure and from the 50S subunit structure results in a phosphorus atom r.m.s. deviation of 5.2 Å.

The structure of our complex with ASL^{Phe} in the P site, and our inability to crystallize an RRF complex of the 70S ribosome with full-length tRNA, are consistent with the proposal that RRF binds stably to ribosomes with tRNA in a P/E hybrid state^{10,20}. In the P/E state, the anticodon stem-loop is still in the P site of the 30S subunit, as observed in the present structure, but the acceptor arm has moved from the P site to the E site in the 50S subunit. Such a P/E hybrid state is evident in the cryo-EM structure of RRF bound to *E. coli* 70S ribosomes with full-length tRNAs¹².

Recent biochemical studies on the action of viomycin in translocation²⁶ have used fluorescent resonance energy transfer and footprinting to show that the hybrid P/E state of tRNA is related to the ratcheting between subunits upon EF-G binding that has been observed by cryo-EM²⁷. It is likely that RRF has the potential, especially in concert with EF-G, to stabilize a ratcheted form of the ribosome that would be characterized by both a relative rotation of the subunits and a hybrid P/E state of the deacylated tRNA. Such a structure may have altered intersubunit bridges as well as a different conformation of H69, and it could facilitate easier subunit dissociation. Moreover, if, in the presence of full-length P-site tRNA, RRF stabilizes a hybrid state with ratcheted subunits, this would also explain its failure to bind in the present crystal form in the presence of full-length tRNAs, as well as the loss of diffraction from such crystals when RRF was soaked into them. Nevertheless, our structure shows that such conformational changes are neither a requirement for, nor a direct result of, RRF binding to the ribosome.

In conclusion, the structure presented here shows details of the interaction of RRF with the ribosome. Although the overall orientation of RRF is similar to those previously reported in lower-resolution studies, some of the key interactions are different. Moreover, H69, which has been implicated in both RRF binding and translocation, is in a conformation identical to that in the ribosome without RRF. This suggests that any conformational change in H69 is neither a requirement for, nor a necessary effect of, RRF binding. Rather, such changes are likely to be facilitated by the further action of EF-G, which is known

from previous studies to stabilize the ratcheted form of the ribosome²⁷. Recent work has shown this ratcheted form to be related to a hybrid state of the ribosome²⁶. Understanding the exact sequence of conformational changes and the mechanism of recycling by RRF and EF-G will require further studies. Our work also shows that, in principle, it is possible to carry out crystallographic studies of complexes of whole ribosomes with translation factors at moderately high resolution.

METHODS

Ribosomes, mRNA and tRNAs. *Thermus thermophilus* 70S ribosomes and tRNA^{Met} were purified as described^{21,28,29}. The mRNA and ASL^{Phe} oligonucleotides were chemically synthesized (Dharmacon) and deprotected as specified by the manufacturer. The sequence of mRNA used is 5'-GAGGAGG ACGGAGAUUGUUCUAGUACAAUAAU-3' (the codons for fMet, Phe and stop are underlined), and that of ASL^{Phe} is 5'-GGGGAUUGAAAAUCCCC-3' (anticodon is underlined).

RRF purification. The RRF gene from *T. thermophilus* was cloned between the NdeI and Sall sites of the T7 vector pET42b (Novagen), which results in a short C-terminal His tag. Expression in the *E. coli* strain BL21(DE3) pLysS was induced with IPTG at an A₆₀₀ of 0.5–0.7. Cells were resuspended in 10 ml buffer A per 10 g of cells (buffer A: 50 mM Tris-HCl (pH 7.5), 200 mM KCl, 1 mM β-mercaptoethanol, 1 tablet of Roche complete EDTA-free protease inhibitor cocktail per 50 ml of buffer and 0.1 mM benzimidazole, with 0.5 mM phenylmethylsulfonyl fluoride added just before use) and disrupted by sonication. Cell debris was pelleted by centrifugation in a Sorvall SS34 rotor for 0.5 h at 16,000 r.p.m. The supernatant was heated to about 65 °C for 20 min and denatured proteins were pelleted by another centrifugation step as described above. The supernatant was filtered through a 0.2-μm filter, loaded on a nickel Fast-Flow column and eluted with a linear gradient into buffer A plus 200 mM imidazole. The peak was pooled and the protein concentration was estimated by measuring the A₂₈₀. The protein was precipitated by slow addition of 3 M ammonium sulfate and kept on ice for at least 0.5 h. After centrifugation at 4,500 r.p.m., the pellet was resuspended in a minimal volume of buffer B (20 mM MES-KOH (pH 6.0), 200 mM KCl, 1 mM β-mercaptoethanol) to a final concentration of about 15–20 mg ml⁻¹. The sample was filtered and loaded onto a Superdex 75 column. The peak fractions were pooled and the protein was concentrated to approximately 60 mg ml⁻¹, flash-frozen in liquid nitrogen and stored at –80 °C.

Complex formation. Complexes were formed in buffer G (50 mM KCl, 10 mM NH₄Cl, 10 mM magnesium acetate, 5 mM potassium-HEPES (pH 7.5), 6 mM β-mercaptoethanol). To form a post-termination complex, 4.4 μM 70S ribosomes were programmed with 17.6 μM mRNA and incubated at 55 °C for 5 min, after which 44 μM ASL^{Phe} was added and the complex incubated for 30 min at 55 °C. At this point, 17.6 μM tRNA^{Met} was added and the complex was incubated for an additional 30 min at 55 °C. The complex was then left at room temperature before crystallization. 2.8 mM Deoxy Big Chap (Hampton Research) was added directly before setup of the crystallization screen.

Crystallization. Crystals were set up and grown as described²¹, except that KSCN was varied between 0.1 and 0.2 M. The crystal used in this work was grown in 0.1 M KSCN, 4% (w/v) PEG 20,000, 4% (v/v) PEG 550 MME and 0.1 M Tris-acetate (pH 7). The crystals were transferred in three steps (with 10%, 20% and 30% (v/v) PEG 400, respectively) into the final cryoprotecting solution (0.1 M KSCN, 0.1 M Tris-acetate (pH 7), 4.4% (w/v) PEG 20,000, 4.4% (v/v) PEG 550 MME, 30% (v/v) PEG 400). The final solution contained 200 μM RRF, and crystals were left for 48 h before flash-cooling by plunging into liquid nitrogen. Data collection was carried out at 100 K.

Data collection, refinement and model building. Crystals were prescreened at beamline 14.1 of the Synchrotron Radiation Source, Daresbury Laboratory or at beamlines ID 14-1 and ID 14-3 of the European Synchrotron Radiation Facility (ESRF). Data sets were collected at beamline ID 14-4 at the ESRF. Data were integrated and scaled using the XDS package³⁰.

The structure was refined using CNS version 1.2 (ref. 31), starting with a model of the *T. thermophilus* 70S ribosome²¹, from which ligands and ions were initially excluded. The refinement protocol and application of

Table 1 Data collection and refinement statistics

70S ribosome–RRF complex	
Data collection	
Space group	$P2_12_12_1$
Cell dimensions	
<i>a</i> , <i>b</i> , <i>c</i> (Å)	212.4, 450.1, 630.5
Resolution (Å)	50–3.5
R_{sym}	30.4 (72.8)
$I / \sigma I$	3.8 (1.59)
Completeness (%)	96.7 (88.8)
Redundancy	6.2 (5.7)
Refinement	
Resolution (Å)	20.0–3.5
No. reflections	740,306
$R_{\text{work}} / R_{\text{free}}$	26.5 / 32.6
No. atoms	
RNA	96,714 (per molecule)
Protein	47,337 (per molecule)
Ions	491 (molecule I) + 560 (molecule II)
B-factors	
RNA	84.53
Protein	101.63
Ions	41.94
R.m.s. deviations	
Bond lengths (Å)	0.0069
Bond angles (°)	1.18

Values in parentheses are for data at the outer resolution shell of 3.6–3.5 Å. Although all data measured to 3.5-Å resolution were used for refinement, the value of $I / \sigma I$ dropped below 2.0 at 3.8 Å. At this resolution, the values were $R_{\text{sym}} = 55.9\%$, completeness = 96.2% and redundancy = 6.3.

noncrystallographic restraints were as described²¹. Model building was done in Coot³². A summary of data collection and refinement statistics is shown in **Table 1**.

Accession codes. Protein Data Bank: Coordinates have been deposited with accession codes 2V46, 2V47, 2V48 and 2V49.

Note: Supplementary information is available on the Nature Structural & Molecular Biology website.

ACKNOWLEDGMENTS

We thank F. Murphy for help with data collection during optimization of crystallization conditions, M. MacDonald for help with screening at beamline 14.1 at the Synchrotron Radiation Source, and R. Ravelli, J. McCarthy and G. Leonard at beamlines ID14-1, ID14-3 and ID14-4 at the ESRF for help with screening and data collection. This work was supported by the Medical Research Council (UK), the US National Institutes of Health and the Agouron Institute, and fellowships from the Austrian Academy of Sciences (A.W.), the Boehringer Ingelheim Fonds (S.P.), the American Cancer Society (C.M.D.) and the Wenner-Gren foundation (M.S.).

AUTHOR CONTRIBUTIONS

A.W. crystallized the complex with RRF, collected and analyzed the data and wrote the paper. S.P. and C.M.D. helped with optimization of mRNA constructs, crystallization and cryoprotection conditions, helped with data collection, initial processing and model building, and gave feedback on the manuscript. M.S. cloned, expressed and purified *T. thermophilus* RRF, suggested crystallization of its complex with the ribosome and provided feedback on the manuscript. A.C.K. purified ribosomes and tRNA. V.R. oversaw the work and helped with writing the paper.

COMPETING INTERESTS STATEMENT

The authors declare no competing financial interests.

Published online at <http://www.nature.com/nsmb/>

Reprints and permissions information is available online at <http://npg.nature.com/reprintsandpermissions>

- Hirashima, A. & Kaji, A. Purification and properties of ribosome-releasing factor. *Biochemistry* **11**, 4037–4044 (1972).
- Janosi, L., Shimizu, I. & Kaji, A. Ribosome recycling factor (ribosome releasing factor) is essential for bacterial growth. *Proc. Natl. Acad. Sci. USA* **91**, 4249–4253 (1994).
- Hirashima, A. & Kaji, A. Role of elongation factor G and a protein factor on the release of ribosomes from messenger ribonucleic acid. *J. Biol. Chem.* **248**, 7580–7587 (1973).
- Selmer, M., Al-Karadaghi, S., Hirokawa, G., Kaji, A. & Liljas, A. Crystal structure of *Thermotoga maritima* ribosome recycling factor: a tRNA mimic. *Science* **286**, 2349–2352 (1999).
- Kim, K.K., Min, K. & Suh, S.W. Crystal structure of the ribosome recycling factor from *Escherichia coli*. *EMBO J.* **19**, 2362–2370 (2000).
- Toyoda, T. *et al.* Crystal structure combined with genetic analysis of the *Thermus thermophilus* ribosome recycling factor shows that a flexible hinge may act as a functional switch. *RNA* **6**, 1432–1444 (2000).
- Nakano, H. *et al.* Structure and binding mode of a ribosome recycling factor (RRF) from mesophilic bacterium. *J. Biol. Chem.* **278**, 3427–3436 (2003).
- Yoshida, T. *et al.* Solution structure of the ribosome recycling factor from *Aquifex aeolicus*. *Biochemistry* **40**, 2387–2396 (2001).
- Yoshida, T. *et al.* Characteristic domain motion in the ribosome recycling factor revealed by 15N NMR relaxation experiments and molecular dynamics simulations. *Biochemistry* **42**, 4101–4107 (2003).
- Lancaster, L., Kiel, M.C., Kaji, A. & Noller, H.F. Orientation of ribosome recycling factor in the ribosome from directed hydroxyl radical probing. *Cell* **111**, 129–140 (2002).
- Agrawal, R.K. *et al.* Visualization of ribosome-recycling factor on the *Escherichia coli* 70S ribosome: functional implications. *Proc. Natl. Acad. Sci. USA* **101**, 8900–8905 (2004).
- Gao, N. *et al.* Mechanism for the disassembly of the posttermination complex inferred from cryo-EM studies. *Mol. Cell* **18**, 663–674 (2005).
- Wilson, D.N. *et al.* X-ray crystallography study on ribosome recycling: the mechanism of binding and action of RRF on the 50S ribosomal subunit. *EMBO J.* **24**, 251–260 (2005).
- Rao, A.R. & Varshney, U. Specific interaction between the ribosome recycling factor and the elongation factor G from *Mycobacterium tuberculosis* mediates peptidyl-tRNA release and ribosome recycling in *Escherichia coli*. *EMBO J.* **20**, 2977–2986 (2001).
- Ito, K., Fujiwara, T., Toyoda, T. & Nakamura, Y. Elongation factor G participates in ribosome disassembly by interacting with ribosome recycling factor at their tRNA-mimicry domains. *Mol. Cell* **9**, 1263–1272 (2002).
- Guo, P., Zhang, L., Zhang, H., Feng, Y. & Jing, G. Domain II plays a crucial role in the function of ribosome recycling factor. *Biochem. J.* **393**, 767–777 (2006).
- Hirashima, A. & Kaji, A. Factor-dependent release of ribosomes from messenger RNA. Requirement for two heat-stable factors. *J. Mol. Biol.* **65**, 43–58 (1972).
- Karimi, R., Pavlov, M.Y., Buckingham, R.H. & Ehrenberg, M. Novel roles for classical factors at the interface between translation termination and initiation. *Mol. Cell* **3**, 601–609 (1999).
- Hirokawa, G. *et al.* Post-termination complex disassembly by ribosome recycling factor, a functional tRNA mimic. *EMBO J.* **21**, 2272–2281 (2002).
- Peske, F., Rodnina, M.V. & Wintermeyer, W. Sequence of steps in ribosome recycling as defined by kinetic analysis. *Mol. Cell* **18**, 403–412 (2005).
- Selmer, M. *et al.* Structure of the 70S ribosome complexed with mRNA and tRNA. *Science* **313**, 1935–1942 (2006).
- Maguire, B.A., Beniaminov, A.D., Ramu, H., Mankin, A.S. & Zimmermann, R.A. A protein component at the heart of an RNA machine: the importance of protein I27 for the function of the bacterial ribosome. *Mol. Cell* **20**, 427–435 (2005).
- Yusupov, M.M. *et al.* Crystal structure of the ribosome at 5.5 Å resolution. *Science* **292**, 883–896 (2001).
- Schuwirth, B.S. *et al.* Structures of the bacterial ribosome at 3.5 Å resolution. *Science* **310**, 827–834 (2005).
- Korostelev, A., Trakhanov, S., Laurberg, M. & Noller, H.F. Crystal structure of a 70S ribosome-tRNA complex reveals functional interactions and rearrangements. *Cell* **126**, 1065–1077 (2006).
- Ermolenko, D.N. *et al.* The antibiotic viomycin traps the ribosome in an intermediate state of translocation. *Nat. Struct. Mol. Biol.* **14**, 493–497 (2007).
- Frank, J. & Agrawal, R.K. A ratchet-like inter-subunit reorganization of the ribosome during translocation. *Nature* **406**, 318–322 (2000).
- Petry, S. *et al.* Crystal structures of the ribosome in complex with release factors RF1 and RF2 bound to a cognate stop codon. *Cell* **123**, 1255–1266 (2005).
- Schmitt, E., Panvert, M., Blanquet, S. & Mechulam, Y. Crystal structure of methionyl-tRNA^{Met} transformylase complexed with the initiator formyl-methionyl-tRNA^{Met}. *EMBO J.* **17**, 6819–6826 (1998).
- Kabsch, W. Automatic processing of rotation diffraction data from crystals of initially unknown symmetry and cell constants. *J. Appl. Cryst.* **26**, 795–800 (1993).
- Brünger, A.T. *et al.* Crystallography & NMR system: a new software suite for macromolecular structure determination. *Acta Crystallogr. D Biol. Crystallogr.* **54**, 905–921 (1998).
- Emsley, P. & Cowtan, K. Coot: model-building tools for molecular graphics. *Acta Crystallogr. D Biol. Crystallogr.* **60**, 2126–2132 (2004).